Cite as: S. E. Harrison *et al*., *Science* 10.1126/science.aal1810 (2017).

Assembly of embryonic and extra-embryonic stem cells to mimic embryogenesis in vitro

Sarah Ellys Harrison,[1]* Berna Sozen,[1,2]* Neophytos Christodoulou,[1] Christos Kyprianou,[1] Magdalena Zernicka-Goetz[1]†

[1]Mammalian Embryo and Stem Cell Group, University of Cambridge, Department of Physiology, Development and Neuroscience, Downing Street, Cambridge CB2 3DY, UK.
[2]Department of Histology and Embryology, Faculty of Medicine, Akdeniz University, Antalya, 07070, Turkey.

*These authors contributed equally to this work.

†Corresponding author. Email: mzg@mole.bio.cam.ac.uk

Mammalian embryogenesis requires intricate interactions between embryonic and extra-embryonic tissues to orchestrate and coordinate morphogenesis with changes in developmental potential. Here, we combine mouse embryonic stem cells (ESCs) and extra-embryonic trophoblast stem cells (TSCs) in a 3D-scaffold to generate structures whose morphogenesis is remarkably similar to natural embryos. By using genetically-modified stem cells and specific inhibitors, we show embryogenesis of ESC- and TSC-derived embryos, ETS-embryos, depends on crosstalk involving Nodal signaling. When ETS-embryos develop, they spontaneously initiate expression of mesoderm and primordial germ cell markers asymmetrically on the embryonic and extra-embryonic border, in response to Wnt and BMP signaling. Our study demonstrates the ability of distinct stem cell types to self-assemble in vitro to generate embryos whose morphogenesis, architecture, and constituent cell-types resemble natural embryos.

Early mammalian development requires the formation of embryonic and extra-embryonic tissues and their cooperative interactions. As a result of this partnership, the embryonic tissue, epiblast, will become patterned to generate cells of the future organism. Concomitantly, the extra-embryonic tissues, the trophectoderm and primitive endoderm, will form the placenta and the yolk sac. These embryonic and extra-embryonic tissues become defined before the embryo implants into the uterus as a result of cellular heterogeneity, polarization and position culminating in a blastocyst structure with three distinct cell lineages (*1*).

As the embryo implants, the relatively simple architecture of the blastocyst becomes re-organized in a progressive sequence of spatial and temporal morphogenetic steps into the much more complex architecture of the so-called 'egg cylinder' (Fig. 1a, top) (*2*, *3*). This re-modelling is triggered by dialogue between embryonic and extra-embryonic tissues that initiates integrin-mediated signaling leading the embryonic epiblast cells to polarize, adopt a rosette-like configuration, and then undertake lumenogenesis (*4*). This architectural re-organization of the epiblast is followed by development of the trophectoderm into extra-embryonic ectoderm (ExE) that also forms a cavity. Finally, both embryonic and extra-embryonic cavities unite to form a single pro-amniotic cavity and the embryo visibly breaks its symmetry to initiate mesoderm and primordial germ cell induction (Fig. 1a, top). This key symmetry breaking event occurs at the boundary between embryonic and extra-embryonic tissues and involves Nodal, Wnt and BMP signaling pathways (*5–8*).

As the embryo grows from the blastocyst into the elongated structure of the egg cylinder, the primitive endoderm develops into the visceral endoderm (VE), which becomes regionalised. The distal part of the VE (the distal VE, DVE) expresses inhibitors of the Nodal and Wnt signaling pathways and migrates anteriorly (anterior VE, AVE) to pattern the anterior epiblast (*9–11*). At the posterior, a BMP4 signal from the ExE induces the activity of Wnt and Nodal in the adjacent epiblast. Nodal feeds back positively on BMP, which in turn reinforces Wnt, in a self-sustaining interaction loop (*12–14*). This specifies posterior identity and therefore defines the location for primitive streak formation and mesoderm induction.

Pre-implantation epiblast cells have been established as ESCs that can be maintained indefinitely in culture (*15*, *16*). ESCs retain pluripotency and have the ability to be directed to develop into organoids that present an invaluable system to recapitulate many aspects of organ formation in vitro (*17–22*). Embryoid bodies or micro-patterned colonies developed from ESCs are also a valuable model for development as they can be induced to express genes associated with specification of embryonic lineages using external stimuli (*23–26*). However, although such gene expression can be polarised, the structures formed do not follow the spatial-temporal events of embryogenesis and ultimately do not acquire the characteristic architecture of a post-

implantation embryo. We hypothesized that this is because in these systems, ESCs develop with a drastically different number and spatial organization of cells and, in addition, lack signals from the extra-embryonic tissues that guide embryo development upon implantation. Here we test this hypothesis by taking advantage of our recent understanding of the steps involved in the embryonic/extra-embryonic interactions during implantation and early post-implantation development (*4*) and trying to mimic them in stem cells developing in vitro.

Experimental strategy

Our strategy was to attempt to use embryonic and extra-embryonic stem cells to replicate the spatial and temporal sequence of events of mouse embryogenesis in vitro (*4*). To achieve this, we used single ESCs and small clumps of TSCs (*27*) and developed a culture system which would enable their interaction within a three-dimensional (3D) scaffold of extra-cellular matrix (ECM) in a medium which composition (see Methods) allows both ESCs and TSCs co-develop, which we created for this purpose (Fig. 1a, bottom). We hypothesized that 3D scaffold of ECM in Matrigel would be able to substitute for the primitive endoderm by providing ECM essential for epiblast polarisation and lumenogenesis. We found that in these culture conditions ESCs and TSCs developed into an elongated cylindrical architecture typical of the post-implantation mouse embryo (Fig. 1b-c; fig. S1a). Careful examination of morphology, size, cell numbers, and expression of lineage markers revealed discrete ESC- and TSC-derived compartments within a single cylindrical structure with a central cavity that was remarkably similar to post-implantation embryos developing either in vitro or in vivo (Fig. 1b-g, fig. S1b,c). By determining the expression of a typical primitive endoderm marker, Gata4, we confirmed that the formation of these embryo-like structures did not involve the presence of primitive endoderm (Fig. 1h).

Development of these ESC- and TSC-derived structures was highly reproducible: in a typical 3D culture, 22% of all structures comprised both ESCs and TSCs; 61% were built only from ESCs and 17% only from TSCs (Fig. 1i,j; n=400). Of all structures comprising ESCs and TSCs, most (92.68%, n=88) had the characteristic cylindrical architecture with single adjoining ESC and TSC compartments whereas the remaining 7.32% had two ESC compartments occupying polar positions in relation to a single TSC compartment (Fig. 1k). These results indicate that ESCs and TSCs cultured in 3D scaffold of ECM have the ability to self-assemble an embryo architecture, leading us to term these ESC- and TSC-derived embryos, ETS-embryos.

Pro-amniotic cavity formation in ETS-embryogenesis

The first critical morphogenetic event in post-implantation embryogenesis is pro-amniotic cavity formation. We therefore wished to determine whether a similar morphogenetic event could take place in ETS-embryos. During mammalian embryogenesis, the embryonic cavity has been recently discovered to form not through cell death, as previously thought, but through apical cellular constriction followed by lumenogenesis (*4*, *28*). To gain insight into the cavitation of ETS-embryos, we examined the localization of a cell adhesion marker (E-cadherin) at sequential time-points in development (Fig. 2a-c; fig. S2). After 72 hours of plating, only a single cavity could be detected in ETS-embryos and it was present in the ESC-compartment (Fig. 2a). By 84 hours, one or more small additional cavities developed within the TSC-compartment (Fig. 2b, fig.S2). Finally, by 96 hours, the cavities in ESC and TSC compartments united into a single large cavity (Fig. 2c, fig. S2). These observations demonstrate that a cavity first forms in the ESC-derived embryonic compartment, ahead of cavitation in the TSC-derived extra-embryonic compartment and they finally become united into a single cavity spanning the whole cylindrical structure by 96 hours after stem cell plating (Fig. 2c).

To support these observations, we also examined the distribution of the transmembrane protein Podocalyxin (PCX) together with a marker of apical polarity, aPKC (Fig. 2d-f), in the ESC and TSC compartments of ETS-embryos as their development progressed. PCX is a negatively-charged silomucin which accumulates on the apical sides of epiblast cells during pro-amniotic cavity formation (*4*). In agreement with these observations in embryos, we detected the accumulation of PCX along the apical sides of the cells in the ESC compartment when a single lumen was present at 72 hours (Fig. 2d, 2g). In contrast, no such accumulation around a cavity was evident in the TSC compartment at this stage (Fig. 2d, 2g). By 84 hours, PCX was also seen to accumulate on the apical sides of cells in the TSC compartment as multiple individual cavities emerged in this compartment (Fig. 2e, 2h). After 96 hours of development, these ESC and TSC cavities had unified and PCX lined a central, common cavity and was concentrated at the apical sides of cells in both compartments (Fig. 2f-i). This sequence of events is similar to pro-amniotic cavity formation during natural embryogenesis (*4*, *28*). We observed a mean of 2 dying cells per ESC and TSC compartment, which is a similar incidence of cell death to that we could detect in natural embryos (fig. S3a-e). The site of cell death in ETS-embryos had no relationship to the ESC or TSC cavitation or ESC-TSC border, suggesting that apoptosis is not a likely driver behind cavity formation and unification, similar to natural embryogenesis (fig. S3a-e).

How the embryonic and extra-embryonic cavities unite during embryo development is currently unknown (*4*). Encouraged by our finding of a similar distribution of PCX

during natural and ETS-embryogenesis at the time of cavity formation and unification (Fig. 3a-b), we sought to use the ETS-embryo model to gain insight into how a cavity might develop at the embryonic-extra-embryonic interface. Before a continuous cavity formed, the shapes of TSCs at the ESC-TSC border differed significantly from columnar morphology of non-border cells (fig. S4a-b). Before cavities merged together, a basement membrane (marked by laminin staining) between the compartments was detectable (Fig. 3c, 72 hours, left). This distribution of laminin was similar to the basement membrane present between embryonic and extra-embryonic compartments of the E4.75 embryo (Fig. 3d, left and inset). As ETS-embryos underwent cavitation, the laminin boundary became broken (Fig. 3c, 84 hours; Fig. 3e), which mirrored the breakdown of the basement membrane during egg cylinder morphogenesis in vivo (Fig. 3d, middle). In both the ETS-embryo and the natural embryo, full expansion of the cavity across embryonic and extra-embryonic compartments led to the complete disappearance of the basement membrane between compartments (Fig. 3c, 96 hours, Fig. 3d, right). During ETS-embryogenesis, the laminin boundary was displaced toward the TSC compartment whereas, in contrast, when two structures comprised of only ESCs fused together, laminin was not displaced in any particular direction, suggesting that laminin displacement toward the extra-embryonic compartment is a characteristic of the ESC-TSC junction (Fig. 3c, far-right; Fig. 3e). Concomitant with laminin displacement, we also noted formation of rosette-like chimeric cell arrangements comprising both ESCs and TSCs during cavitation of ETS-embryos (Fig. 3f-g). We found that epiblast and ExE cells adopt very similar cell arrangements at the boundary between compartments in natural embryos (Fig. 3h), which might be involved in the unification of cavities during pro-amniotic cavity formation. These results reveal the sequence of events leading to embryonic and extra-embryonic cavity unification during ETS-embryogenesis and suggest that similar cell-rearrangements occur in the natural embryogenesis, to facilitate morphogenesis, as also proposed in other models of epithelialization and branching (*29*).

Role of Nodal signaling during ETS-embryogenesis

Although TSCs developing together with ESCs cavitate, the great majority of TSCs developing on their own do not cavitate within the same frame of time (Fig. 4a-c), suggesting that the ESC compartment might signal to promote development of the TSC compartment. One candidate for such signaling would be Nodal/Activin, which is known to be secreted by ESCs (*30*) and to be essential for early post-implantation development (*5*, *31*, *32*). Moreover, Nodal/ Activin signaling is required for TSC renewal in culture, and in conventional culture conditions is provided by mouse embryonic fibroblast (MEF) feeder cells or exogenously in the medium (*33–35*). Since our culture conditions contain neither of these components, we hypothesized that the ESC compartment might be providing the Nodal/Activin signal required for development of TSCs into the extra-embryonic-compartment. Since the earliest role of Nodal signaling is difficult to probe in Nodal knock-out embryos due to the presence of Nodal protein in the reproductive tract (*36*), we used ETS-embryogenesis to gain insight into the role of Nodal/Activin in the process of building the embryo-like structure. We generated ETS-embryos in the presence of the Activin/TGF-beta receptor inhibitor, SB431542 (*37*), which was added to the culture 48 hours after cell plating (Fig. 4d, middle). We verified the inhibition of the Nodal/Activin pathway by assessing phosphorylation of SMAD2 (Fig. 4d, middle), and interrogated PCX staining intensity profiles in different compartments of ETS-embryos to verify cavitation. Although a significant majority of control ETS-embryos developed a cavity in the TSC compartment, in the presence of 10μm SB431542, the TSC compartment failed to cavitate in a significant majority of ETS-embryos (90% versus 30%, $P<0.01$, Fisher's exact test; n=10 in both groups, Fig. 4d, 4f, left), whereas cavitation within the ESC compartment was unaffected, although we noted a reduction in Oct4 expression (Fig. 4d, middle). To further dissect the role of Nodal/Activin signaling in the development of the TSC compartment, we generated ETS-embryos using tamoxifen inducible-knockout Nodal ESCs (*38*). Similar to the effect of SB-treatment, we found that the TSC compartment failed to cavitate in the majority (80%, $P<0.05$, Fisher's exact test; n=10) of Nodal−/−ESC ETS-embryos (Fig. 4d, bottom; 4f, left). Since these results indicated a role of the embryonic compartment and Nodal/Activin signaling in the development of the extra-embryonic compartment, we wished to test whether this might also be so in natural embryos. We recovered embryos just before cavitation in the ExE, at E5.0, and cultured them for 36 hours in the presence of 10μM SB431542 (Fig. 4e bottom). We found that as with ETS-embryos, the ExE in the majority (90%, $P<0.05$, Fisher's exact test; n=10) of SB-treated embryos failed to cavitate, whereas the majority of control embryos cavitated (85%, $P<0.05$, Fisher's exact test; n=14) (Fig. 4e, 4f right). Cavitation within the embryonic compartment was unaffected although there was a reduction in Oct4 expression (Fig. 4e), similarly to what we observed in ETS-embryos (Fig. 4d). In agreement with these data, addition of exogenous Activin to TSCs cultured without ESCs allowed cavitation (Fig. 4g; 70%, $P<0.001$, Fisher's exact test; n=20). Together, these experiments suggest a role of the embryonic compartment, and specifically Nodal/Activin signaling, in supporting the development of the extra-embryonic compartment in ETS- and natural embryos developing through early post-implantation stages.

Generation of regionalized mesoderm during ETS-embryogenesis

Once the pro-amniotic cavity has formed, the next major developmental step is the breaking of the embryo's symmetry to specify the site of germ layer formation. In natural embryogenesis this is known to involve cooperation between the trophectoderm-derived ExE, which signals development of posterior structures, and the primitive endoderm-derived DVE and AVE, which repress posterior signals (*2*). To determine whether ETS-embryos, which lack DVE and AVE, could initiate an asymmetric expression of germ layer markers, we examined if they can progress in their development to express *T/Brachyury*, a mesoderm marker (*39*, *40*). In these experiments we used ESCs that express a *T:GFP* reporter to monitor *T/Brachyury* expression (*41*). We found that from 96 hours of development, the ETS-embryos expressed *T:GFP*, in a domain that was confined to one side of the ESC compartment extending from the boundary with the TSC compartment (Fig. 5a). To address whether this induction of *T:GFP*expression in ESC compartment was promoted by the neighboring TSC compartment, we also generated structures comprising ESCs only, and let them develop under the same conditions and for the same period of time. A significantly higher proportion of ETS-embryos expressed *T:GFP* than the structures comprised of only ESCs (Fig. 5a,b). We also observed that a significantly higher proportion of ESCs developing together with TSCs during ETS-embryogenesis expressed *T:GFP* asymmetrically in comparison to structures comprised of only ESCs (Fig. 5c). To quantitatively assess the asymmetry of *T* expression in relation to the axes of the whole structure, we plotted the coordinates of every single cell expressing *T* upon a projection of all cells in the structure and used Fisher's exact test to determine whether a cell's position was related to its propensity to express *T* (Fig. 5d-f). As a proof-of-principle, we performed similar analyses on E6.5 embryos recovered from the mother (Fig. 5g-i). Such measurements in both ETS- and natural embryos revealed highly regionalised induction of *T* expression. To confirm the identity of T-expressing cells as mesoderm lineage, we analyzed the expression level of another two mesodermal markers, *Mixl1* and *Hand1*. We found significantly increased expression of transcripts of both of these markers, as well as *T*, in T:GFP-positive cells when compared to T:GFP-negative ESCs at opposite site of the ETS-embryo (Fig. 5j, top row). These T:GFP-positive cells also expressed elevated levels of the transcription factor *Snai1* and the intermediate filament protein *Vimentin* which are both expressed in mesenchymal cells, suggesting that cells in the mesodermal region were undergoing comparable cellular changes to cells initiating mesoderm formation in the E6.5 embryo (Fig. 5j, middle).

RT-qPCR analysis of cells in the ESC compartment opposite the mesodermal region revealed that they expressed markers known to be expressed in the region opposite mesoderm specification in the E6.5 embryo (Fig. 5j, bottom) (*42*, *43*). We also observed an opposing gradient of expression of Oct4 and T:GFP across the embryonic compartment (Fig. 5k), as is known to occur from anterior to posterior in the embryo (*44*). Additionally, the mesodermal region which became specified in ETS-embryos occupied a similar proportion of the ESC-derived embryonic compartment when compared with natural embryos of a comparable stage (Fig. 5l). These results indicate that the TSC compartment is able to induce regionalised expression of mesoderm markers in a manner mimicking the ExE in the embryo.

In normal embryogenesis, Wnt3 expression precedes the induction of mesoderm (*6*). To test whether Wnt signaling might also be required to initiate expression of mesoderm markers in the ETS-embryogenesis, we generated ETS-embryos using H2B-GFP:Tcf/LEF reporter ESCs (*45*) and monitored Wnt signaling activity. After 90 hours, localized expression of H2B-GFP:Tcf/LEF could be detected at the ESC-TSC boundary, but *T/Brachyury* was not expressed at that time (Fig. 6a, left). However, when we cultured ETS-embryos for an additional 6 hours, expression of H2B-GFP:Tcf/LEF co-localized with expression of *T/Brachyury* (Fig. 6a, center). This domain of T/Brachyury and H2B-GFP:Tcf/LEF-expressing cells increased in number and size over the next 6 hours (Fig. 6a right, 6b), indicating that canonical Wnt signaling precedes mesodermal specification. In order to determine whether Wnt signaling is also essential for mesodermal specification, we generated ETS-embryos and then let them develop in the presence of the canonical Wnt antagonist DKK1 (*46*), which was added after 48 hours of culture. In contrast to controls, the proportion of ETS-embryos specifying mesoderm was significantly reduced after 96 hours (38% of controls expressed T, whereas only 4% of structures treated with DKK1 did so, Student's *t* test $P<0.001$, $n=100$; Fig. 6c-d). These results indicate that Wnt signaling is crucial to induce the expression of mesoderm markers during ETS-embryogenesis, as is the case in natural embryogenesis.

Specification of primordial germ cell-like cells in ETS-embryogenesis

The next major step in embryogenesis is the specification of primordial germ cells (PGCs). In vivo, PGCs are specified at the boundary between embryonic and extra-embryonic compartments, at the proximal end of the mesodermal domain (*47*). To test whether ETS-embryogenesis is able to lead to PGC-like cell specification, we generated ETS-embryos and let them develop beyond mesoderm specification and examined expression of several markers including *Stella*, *Prdm14*, *Tfap2c (AP2γ)*,*Nanos3, Ddx4* and *Dnmt3b*

(*48*). After 120 hours in culture, we could identify a small cluster of Tfap2c-Oct4 double-positive cells in the ESC compartment, at the ESC-TSC boundary, where *T* was expressed (Fig. 7a). This is a similar site to the location of PGC formation in vivo (*47*, *48*). To confirm this result, we next generated ETS-embryos using ESCs that express GFP-tagged Stella (*Stella:GFP*) (*49*). In accord with our earlier observations, we found a small domain of Stella:GFP expression after 120 hours in culture (Fig. 7b). To investigate the precise location of these putative-PGCs-like cells, we plotted the coordinates of every single cell expressing either of these two PGC markers upon a projection of all cells in the structure. This revealed an average of 5 Tfap2c-Oct4 double-positive and 5 Stella:GFP cells at the boundary between the ESC and TSC compartments (Fig. 7c,d). The precise location of Stella-GFP positive cells at the boundary between compartments contrasted to Stella-GFP expression in structures comprised of ESCs alone, which was distributed in a disorganized manner (fig. S5a, b). To further investigate gene expression characteristic of PGCs, we collected T:GFP positive and negative cells from the ETS-embryos (at the boundary with the extra-embryonic compartment) and performed RT-qPCR analysis. This revealed, as expected for PGCs, upregulated expression of all PGC-marker genes examined: *Tfap2c, Stella, Prdm14, Nanos3, Ddx4* and downregulation of *Dnmt3b* when compared with T:GFP-negative cells outside this region (Fig. 7e). These results indicate that ETS-embryos have the potential to specify PGC-like cells at the boundary between embryonic and extra-embryonic compartments, as natural embryos.

Specification of PGCs during embryogenesis is induced by BMP signaling from the extra-embryonic compartment (*47*). We therefore hypothesized that BMP signaling might play a similar role in the ETS-embryo model. To test this hypothesis, we first confirmed phosphorylation of SMAD1 in ETS-embryos, as in natural embryos, indicating their competence to specify PGCs (Fig. 7b, 7f top, fig. S6a, S6b). We then used ETS-embryogenesis to generate ETS-embryos and let them develop in the presence of Noggin, known to inhibit BMP signaling (*50*), which we confirmed (Fig. 7f). Upon BMP inhibition, a significant majority of ETS-embryos (93%, n=15) failed to express *Stella:GFP*, in contrast to control ETS-embryos (60%, $P<0.005$, Fisher's exact test, n=15; fig. S6c). Finally, we wished to examine whether Wnt signaling is also necessary for induction of expression of PGCs markers during ETS-embryogenesis. To this end, we generated ETS-embryos and treated them with DKK (200ng/ml) after 48 hours of culture. This treatment significantly downregulated expression of PGC marker genes and *T* in ESCs-derived embryonic compartment on the boundary with the TSC-derived compartment, which would undergo PGC specification in control IVEs (Fig. 7g-h). We verified that the Wnt signaling pathway was downregulated by analyzing the expression of *Axin1* and *Wnt3* (Fig. 7g). These results indicate that following the induction of expression of mesoderm markers, ETS-embryogenesis progresses to induce expression of PGC markers in a similar manner to natural embryogenesis.

Discussion

At the onset of our study, we hypothesized that development of a stem cell model of mammalian embryogenesis might require mimicking the complex spatio-temporal sequence of morphogenetic steps occurring during natural embryogenesis. Our recent work allowed us to reveal the sequence of these morphogenetic steps at the time of implantation and early post-implantation development (*3*, *4*). Here we take advantage of this knowledge and show that by fostering close interactions between embryonic and extra-embryonic stem cells in a 3D scaffold of ECM and medium in which they can co-develop, ESCs and TSCs self-assemble into a structure whose development and architecture is very similar to the natural embryo. This in vitro embryogenesis can be broken down into a sequence of five key steps in the development of mammalian embryos from implantation stage to germ layer specification: (1) the spontaneous self-organization leading to polarization and then epithelization and lumenogenesis first in the embryonic (ESC) and then cavitation in the extra-embryonic (TSC) compartments; (2) the unification of embryonic and extra-embryonic cavities into the equivalent of the embryo's pro-amniotic cavity; (3) the crosstalk between embryonic and extra-embryonic compartments, involving Nodal signaling, that builds characteristic embryo architecture; (4) the self-organization of embryonic and extra-embryonic compartments resulting in asymmetric induction of the localized expression of mesoderm markers at the compartment boundary in a Wnt-dependent manner; and (5) the provision of BMP signaling to specify the PGC-like cells, equivalent to their formation in the embryo. These morphogenetic events follow similar spatio-temporal dynamics during ETS-embryogenesis as they do in natural embryogenesis (Fig. 8).

Our studies demonstrate that stem cell-derived ETS-embryos can mimic formation of the embryo's structure and gene expression pattern more accurately than has been possible before using structures derived from ESCs only, such as embryoid bodies (*23–26*). There are three critical differences between the ETS-embryos we describe here and embryoid bodies: the former are built from fewer starting numbers of cells to closely resemble cell numbers in the implanting embryo; they are cultured in a 3D scaffold of ECM as epiblast cells within the embryo; and the ESCs are developing in coordination with TSCs as epiblast cells with trophectoderm cells within the embryo. Our previous stud-

ies showed that a small number of ESCs cultured in ECM were able to organize themselves into a rosette that undergoes lumenogenesis in a manner resembling the natural embryogenesis (*4*). We show here that these ESC-derived rosettes can develop further to spontaneously, i.e without provision of a specific external signal, induce mesoderm gene expression. However, we also now show that achieving robust mesoderm induction that, importantly, respects the embryo's architecture, is fostered by the addition of interactions with extra-embryonic stem cells.

These results point to a remarkable ability of ESCs to pattern due to their interactions with TSCs alone, without a requirement for primitive endoderm-derived structures. This might be because we partially substitute for the primitive endoderm function by providing ECM in the 3D scaffold. In agreement with this hypothesis, we have recently shown that ECM proteins are able to substitute for primitive endoderm to induce epiblast remodeling at the time of implantation (*4*). However, the induction of asymmetric expression of mesoderm and PGC markers during ETS-embryogenesis was surprising to us because during natural embryogenesis, primitive endoderm-derived DVE and AVE provide inhibitors to restrict posterior gene-expression upon their migration anteriorly (*8–11*). The lack of noticeable asymmetry in pSMAD2 in ETS-embryos could be due to the absence of DVE/AVE but, irrespective of this, our results demonstrate that without the localized provision of antagonists, ETS-embryos break symmetry to induce regionalized, asymmetric expression of mesoderm and PGC markers. We hypothesize that this is either due to a random event or an earlier asymmetric morphogenetic step such as the cell re-arrangements that occur during the cavity fusion. Indeed, such re-arrangements could potentially reposition signaling receptors to sense and transduce signals from the neighboring compartment not entirely symmetrically. Regardless of the route by which this is achieved, we further hypothesize that a secretion of an inhibitory signal might act to restrict mesoderm gene expression in adjacent regions. It will be interesting to shed more light on this process in future and, in addition, to determine whether incorporating primitive endoderm stem cells (*51*, *52*) into the ETS-embryogenesis model would extend the developmental potential of this model.

In conclusion, we demonstrate that enabling crosstalk between embryonic and extra-embryonic stem cells in a 3D ECM scaffold is sufficient to trigger self-organization recapitulating spatio-temporal events leading to construction of embryo architecture and patterning. This stem cell model of mammalian embryogenesis, in combination with genetic manipulations, might provide a potentially powerful platform to dissect physical and molecular mechanisms that mediate this critical crosstalk during natural embryogenesis.

Materials & Methods

Embryo recovery and culture

6-week old F1 female (CBAxC57BL/6) mice were naturally mated and sacrificed at midnight (E5.0) or midday (E5.5) after 5 days post-coitum. The uterus was recovered and embryos were dissected from deciduae in M2 medium and cultured as described previously (*53*). Blastocysts were recovered from the mother at E4.5 by uterine flushing. Recovered blastocysts had their mural trophectoderm dissected away, before plating in μ-plates (Ibidi) and cultured in IVC1 and IVC2 media (Cell Guidance Systems).

Embryo immunostaining

Embryos were fixed in 4% paraformaldehyde for 20 min at room temperature, washed twice in PBT (PBS plus 0.05% Tween-20) and permeabilized for 15 min at room temperature in 0.3% Triton-X-100, 0.1% Glycin. Primary antibody incubation was performed overnight at 4°C in blocking buffer (PBS plus 10% FBS, 1% Tween-20). The following day, embryos were washed twice in PBT, then incubated overnight in secondary antibody in blocking buffer at 4°C. On the third day, embryos were washed twice in PBT and incubated for 1 hour at room temperature in DAPI plus PBT (5mg/ml). Embryos were mounted in DAPI plus PBT prior to confocal imaging. For antibodies used, see Supplementary table S1.

Cell culture

ESCs were cultured at 37°C and 5% CO_2 on gelatinized tissue-culture grade plates and passaged once they reached confluency. Cells were cultured in DMEM with 15% FBS, 2mM L-glutamine, 0.1mM 2-ME, 0.1mM NEAA, 1mM sodium pyruvate, and 1% penicillin-streptomycin) supplemented with PD0325901 (1μM), CHIR99021 (3μM) (2i) and leukaemia inhibitory factor (0.1mM, LIF).

TSCs were cultured at 37°C and 5% CO_2, in RPMI 1640 (Sigma) with 20% FBS, 2mM L-glutamine, 0.1mM 2-ME, 1mM sodium pyruvate, and 1% penicillin-streptomycin, plus FGF4 (Peprotech) and heparin (Sigma) in the presence of inactivated DR4 MEFs (*54*). Cells were passaged at 80% confluency.

Cell lines used in the study

All experiments were performed using E14 or 129 mouse ESCs, CAG-GFP ESCs (*55*), Inducible Nodal knockout ESCs (*38*), T:GFP ESCs (*41*), H2B-GFP:Tcf/LEF ESCs (*45*), Stella:GFP ESCs (*49*), and wild-type TSCs.

'3D embedded' culture

ESC colonies were dissociated to single cells, and TSC colonies dissociated into small clumps by incubation with 0.05% trypsin-EDTA at 37°C. Cells were pelleted by centrifugation

for 5 min/1,000 rpm, washed with PBS, and re-pelleted. This was repeated twice, then ESC and TSC suspensions were mixed and re-pelleted. The pellet was re-suspended in Matrigel (BD, 356230). The cell suspension was plated on μ-plates (Ibidi) and incubated at 37°C until the Matrigel solidified. Cells were cultured at 37°C and 5% CO_2. ETS-embryo medium was as follows: 50% RPMI, 25% DMEM F-12 and 25% Neurobasal A supplemented with 10% FBS, 2mM L-glutamine, 0.1mM 2ME, 0.5mM sodium pyruvate, 0.25x N2 supplement, 0.5x B27 supplement, or SOS supplement (Cell Guidance Systems Ltd, Cambridge) FGF4 (12.5 ng/ml) and heparin (Sigma) 500ng/ml (ETS-Embryo medium, ETM, Cell Guidance Systems Ltd, Cambridge). For some experiments, cells were plated using a 3D 'on top' protocol (*56*).

Cell immunostaining

Cells were fixed with 4% paraformaldehyde for 15 min at room-temperature, then rinsed twice in PBS. Permeabilization was performed with 0.3% Triton-X-100, 0.1% Glycin in PBS for 10 min at room-temperature. Primary antibody incubation was performed overnight in blocking buffer (as above) at 4°C. The following day, cells were washed twice in PBS, then incubated overnight in secondary antibody in blocking buffer (as above) at 4°C. DAPI in PBS (5mg/ml) was added prior to confocal imaging. For antibodies used, see Supplementary table S1.

Imaging, processing and analysis

All images were acquired using a Leica SP5 confocal microscope, using a 40x oil-immersion objective. All analyses were carried out using open-source image analysis software 'Fiji' or 'Bioemergences' software (*57*).

Estimation of tissue volume

Tissue volume for ETS-embryos and natural embryos was estimated under the assumption that both ETS-embryos and natural embryos were approximately cylinder shaped. The length and radius of each compartment was measured using image analysis software, then the volume of the cylinder was calculated from these measurements as $V = \pi r^2 l$.

Assessment of cells at the embryonic-extra-embryonic boundary

Cells were classified as lying on the embryonic-extra-embryonic boundary if they had 'nearest neighbor' cells within a 20μm linear distance which were both an ESC and a TSC.

Measurement of laminin displacement angle

Using image analysis software, a line was drawn from ESC compartment to TSC compartment at the middle Z-section of a confocal acquisition of a ETS-embryos. A second line across the boundary was drawn perpendicular. The angle of laminin displacement was then measured relative to these lines. Laminin adjacent to the boundary would therefore have an angle of 90°. Θ is equal to the angle of the laminin extending into the TSC compartment ($\Theta < 90°$).

Assessment of asymmetric gene expression

A line corresponding to the long axis, equivalent to the 'midline' of a ETS-embryo (perpendicular to the embryonic-extra-embryonic boundary) was drawn using image analysis software. At each Z-step, the number of cells positioned either side of this line which expressed the marker-of-interest was counted. If >70% of cells were found to lie on one side of this line, then expression was judged to be asymmetric. In some cases, this method was verified by pointing all cells in a structure using 'Bioemergences' image analysis software ('MovIT') and recording their x, y, and z coordinates. Coordinates of cells expressing the marker-of-interest were also recorded. The long axis, corresponding to the 'midline' was determined from the median coordinates in each dimension, and all coordinates data were run through an R script (*58*) which grouped cells according to their position relative to the long axis/ midline and whether they expressed the marker of interest. A Fisher's exact test was performed to determine if position relative to the long axis was related to expression of the gene by comparing the distribution of the data to the binomial.

Estimation of proportional area of mesodermal regions in ETS-embryos and E6.5 embryos

Image analysis software was used to measure the area occupied by T-positive, mesodermal cells at the middle z-section of confocal acquisition data for ETS-embryos and E6.5 embryos. The total area of the embryonic region was also measured in this way in each case. The ratio was calculated as: Total area of embryonic region/ total area of mesodermal (T-positive) region in each case.

Cell isolation and qRT–PCR

For analysis in fig. S1b, ESC and TSC compartments were collected separately in lysis buffer and RNA was extracted. For analysis of T:GFP-positive cells and opposite T:GFP negative cells in Fig. 5j, 7e and 7g, ETS-embryos were treated briefly with an Enzyme Free Hanks'-Based Cell Dissociation Buffer for 2 min to remove the Matrigel, then had their TSC-compartment dissected away. The ESC compartment was dissociated to single cells by incubation with 0.05% trypsin-EDTA at 37°C. On average 15-20 GFP positive and negative cells were collected separately under a fluorescent microscope and transferred into lysis buffer (Life Technologies). Total RNA was extracted using the Arcturus Pico Pure RNA Isolation Kit and qRT–PCR was performed using the

Power SYBR Green RNA-to-CT 1-Step Kit (Life Technologies) and a Step One Plus Real-time PCR machine (Applied Biosystems). The amounts of mRNA were measured using SYBR Green PCR Master Mix (Ambion). Relative levels of transcript expression were assessed by the ΔΔCt method, with Gapdh as an endogenous control. For qPCR primers used, see Supplementary table S2.

Statistics

Statistical tests were performed on GraphPad Prism 7.0 software for Windows (*59*). Data were checked for normal distribution and equal variances before each parametric statistical test was performed. If appropriate, data were normalised using a square-root transformation. Where appropriate, *t* tests were performed with Welch's correction if variance between groups was not equal. ANOVA tests were performed with a Geisser-Greenhouse correction if variance between groups was not equal. Error bars represent standard error of the mean in all cases, unless otherwise specified. Figure legends indicate the number of independent experiments performed in each analysis.

REFERENCES AND NOTES

1. C. Y. Leung, M. Zernicka-Goetz, Mapping the journey from totipotency to lineage specification in the mouse embryo. *Curr. Opin. Genet. Dev.* **34**, 71–76 (2015). doi:10.1016/j.gde.2015.08.002 Medline
2. S. J. Arnold, E. J. Robertson, Making a commitment: Cell lineage allocation and axis patterning in the early mouse embryo. *Nat. Rev. Mol. Cell Biol.* **10**, 91–103 (2009). doi:10.1038/nrm2618 Medline
3. I. Bedzhov, S. J. L. Graham, C. Y. Leung, M. Zernicka-Goetz, Developmental plasticity, cell fate specification and morphogenesis in the early mouse embryo. *Philos. Trans. R. Soc. B* **369**, 20130538 (2014). doi:10.1098/rstb.2013.0538 Medline
4. I. Bedzhov, M. Zernicka-Goetz, Self-organizing properties of mouse pluripotent cells initiate morphogenesis upon implantation. *Cell* **156**, 1032–1044 (2014). doi:10.1016/j.cell.2014.01.023 Medline
5. J. Brennan, C. C. Lu, D. P. Norris, T. A. Rodriguez, R. S. P. Beddington, E. J. Robertson, Nodal signalling in the epiblast patterns the early mouse embryo. *Nature* **411**, 965–969 (2001). doi:10.1038/35082103 Medline
6. J. A. Rivera-Pérez, T. Magnuson, Primitive streak formation in mice is preceded by localized activation of Brachyury and Wnt3. *Dev. Biol.* **288**, 363–371 (2005). doi:10.1016/j.ydbio.2005.09.012 Medline
7. G. Winnier, M. Blessing, P. A. Labosky, B. L. M. Hogan, Bone morphogenetic protein-4 is required for mesoderm formation and patterning in the mouse. *Genes Dev.* **9**, 2105–2116 (1995). doi:10.1101/gad.9.17.2105 Medline
8. E. J. Robertson, Dose-dependent Nodal/Smad signals pattern the early mouse embryo. *Semin. Cell Dev. Biol.* **32**, 73–79 (2014). doi:10.1016/j.semcdb.2014.03.028 Medline
9. J. A. Belo, T. Bouwmeester, L. Leyns, N. Kertesz, M. Gallo, M. Follettie, E. M. De Robertis, Cerberus-like is a secreted factor with neutralizing activity expressed in the anterior primitive endoderm of the mouse gastrula. *Mech. Dev.* **68**, 45–57 (1997). doi:10.1016/S0925-4773(97)00125-1 Medline
10. M. Yamamoto, Y. Saijoh, A. Perea-Gomez, W. Shawlot, R. R. Behringer, S.-L. Ang, H. Hamada, C. Meno, Nodal antagonists regulate formation of the anteroposterior axis of the mouse embryo. *Nature* **428**, 387–392 (2004). doi:10.1038/nature02418 Medline
11. C. Kimura-Yoshida, H. Nakano, D. Okamura, K. Nakao, S. Yonemura, J. A. Belo, S. Aizawa, Y. Matsui, I. Matsuo, Canonical Wnt signaling and its antagonist regulate anterior-posterior axis polarization by guiding cell migration in mouse visceral endoderm. *Dev. Cell* **9**, 639–650 (2005). doi:10.1016/j.devcel.2005.09.011 Medline
12. N. Ben-Haim, C. Lu, M. Guzman-Ayala, L. Pescatore, D. Mesnard, M. Bischofberger, F. Naef, E. J. Robertson, D. B. Constam, The nodal precursor acting via activin receptors induces mesoderm by maintaining a source of its convertases and BMP4. *Dev. Cell* **11**, 313–323 (2006). doi:10.1016/j.devcel.2006.07.005 Medline
13. P. P. L. Tam, D. A. Loebel, Gene function in mouse embryogenesis: Get set for gastrulation. *Nat. Rev. Genet.* **8**, 368–381 (2007). doi:10.1038/nrg2084 Medline
14. A. Kumar, M. Lualdi, G. T. Lyozin, P. Sharma, J. Loncarek, X.-Y. Fu, M. R. Kuehn, Nodal signaling from the visceral endoderm is required to maintain Nodal gene expression in the epiblast and drive DVE/AVE migration. *Dev. Biol.* **400**, 1–9 (2015). doi:10.1016/j.ydbio.2014.12.016 Medline
15. M. J. Evans, M. H. Kaufman, Establishment in culture of pluripotential cells from mouse embryos. *Nature* **292**, 154–156 (1981). doi:10.1038/292154a0 Medline
16. G. R. Martin, Isolation of a pluripotent cell line from early mouse embryos cultured in medium conditioned by teratocarcinoma stem cells. *Proc. Natl. Acad. Sci. U.S.A.* **78**, 7634–7638 (1981). doi:10.1073/pnas.78.12.7634 Medline
17. T. Sato, R. G. Vries, H. J. Snippert, M. van de Wetering, N. Barker, D. E. Stange, J. H. van Es, A. Abo, P. Kujala, P. J. Peters, H. Clevers, Single Lgr5 stem cells build crypt-villus structures in vitro without a mesenchymal niche. *Nature* **459**, 262–265 (2009). doi:10.1038/nature07935 Medline
18. M. Eiraku, N. Takata, H. Ishibashi, M. Kawada, E. Sakakura, S. Okuda, K. Sekiguchi, T. Adachi, Y. Sasai, Self-organizing optic-cup morphogenesis in three-dimensional culture. *Nature* **472**, 51–56 (2011). doi:10.1038/nature09941 Medline
19. M. A. Lancaster, M. Renner, C. A. Martin, D. Wenzel, L. S. Bicknell, M. E. Hurles, T. Homfray, J. M. Penninger, A. P. Jackson, J. A. Knoblich, Cerebral organoids model human brain development and microcephaly. *Nature* **501**, 373–379 (2013). doi:10.1038/nature12517 Medline
20. Y. Xia, I. Sancho-Martinez, E. Nivet, C. Rodriguez Esteban, J. M. Campistol, J. C. Izpisua Belmonte, The generation of kidney organoids by differentiation of human pluripotent cells to ureteric bud progenitor-like cells. *Nat. Protoc.* **9**, 2693–2704 (2014). doi:10.1038/nprot.2014.182 Medline
21. M. Takasato, P. X. Er, M. Becroft, J. M. Vanslambrouck, E. G. Stanley, A. G. Elefanty, M. H. Little, Directing human embryonic stem cell differentiation towards a renal lineage generates a self-organizing kidney. *Nat. Cell Biol.* **16**, 118–126 (2014). doi:10.1038/ncb2894 Medline
22. C. E. Barkauskas, M. J. Cronce, C. R. Rackley, E. J. Bowie, D. R. Keene, B. R. Stripp, S. H. Randell, P. W. Noble, B. L. M. Hogan, Type 2 alveolar cells are stem cells in adult lung. *J. Clin. Invest.* **123**, 3025–3036 (2013). doi:10.1172/JCI68782 Medline
23. D. ten Berge, W. Koole, C. Fuerer, M. Fish, E. Eroglu, R. Nusse, Wnt signaling mediates self-organization and axis formation in embryoid bodies. *Cell Stem Cell* **3**, 508–518 (2008). doi:10.1016/j.stem.2008.09.013 Medline
24. C. Fuchs, M. Scheinast, W. Pasteiner, S. Lagger, M. Hofner, A. Hoellrigl, M. Schultheis, G. Weitzer, Self-organization phenomena in embryonic stem cell-derived embryoid bodies: Axis formation and breaking of symmetry during cardiomyogenesis. *Cells Tissues Organs* **195**, 377–391 (2012). doi:10.1159/000328712 Medline
25. S. C. van den Brink, P. Baillie-Johnson, T. Balayo, A.-K. Hadjantonakis, S. Nowotschin, D. A. Turner, A. Martinez Arias, Symmetry breaking, germ layer specification and axial organisation in aggregates of mouse embryonic stem cells. *Development* **141**, 4231–4242 (2014). doi:10.1242/dev.113001 Medline
26. A. Warmflash, B. Sorre, F. Etoc, E. D. Siggia, A. H. Brivanlou, A method to recapitulate early embryonic spatial patterning in human embryonic stem cells. *Nat. Methods* **11**, 847–854 (2014). doi:10.1038/nmeth.3016 Medline
27. S. Tanaka, T. Kunath, A.-K. Hadjantonakis, A. Nagy, J. Rossant, Promotion of trophoblast stem cell proliferation by FGF4. *Science* **282**, 2072–2075 (1998). doi:10.1126/science.282.5396.2072 Medline
28. M. N. Shahbazi, A. Jedrusik, S. Vuoristo, G. Recher, A. Hupalowska, V. Bolton, N. M. Fogarty, A. Campbell, L. G. Devito, D. Ilic, Y. Khalaf, K. K. Niakan, S. Fishel, M. Zernicka-Goetz, Self-organization of the human embryo in the absence of maternal tissues. *Nat. Cell Biol.* **18**, 700–708 (2016). doi:10.1038/ncb3347 Medline
29. A. Villasenor, D. C. Chong, M. Henkemeyer, O. Cleaver, Epithelial dynamics of

pancreatic branching morphogenesis. *Development* **137**, 4295–4305 (2010). doi:10.1242/dev.052993 Medline
30. T. Watabe, K. Miyazono, Roles of TGF-beta family signaling in stem cell renewal and differentiation. *Cell Res.* **19**, 103–115 (2009). doi:10.1038/cr.2008.323 Medline
31. D. Mesnard, M. Guzman-Ayala, D. B. Constam, Nodal specifies embryonic visceral endoderm and sustains pluripotent cells in the epiblast before overt axial patterning. *Development* **133**, 2497–2505 (2006). Medline
32. A. Camus, A. Perea-Gomez, A. Moreau, J. Collignon, Absence of Nodal signaling promotes precocious neural differentiation in the mouse embryo. *Dev. Biol.* **295**, 743–755 (2006). doi:10.1016/j.ydbio.2006.03.047 Medline
33. M. Guzman-Ayala, N. Ben-Haim, S. Beck, D. B. Constam, Nodal protein processing and fibroblast growth factor 4 synergize to maintain a trophoblast stem cell microenvironment. *Proc. Natl. Acad. Sci. U.S.A.* **101**, 15656–15660 (2004). doi:10.1073/pnas.0405429101 Medline
34. Y. Ohinata, T. Tsukiyama, Establishment of trophoblast stem cells under defined culture conditions in mice. *PLOS ONE* **9**, e107308 (2014). doi:10.1371/journal.pone.0107308 Medline
35. C. Kubaczka, C. Senner, M. J. Araúzo-Bravo, N. Sharma, P. Kuckenberg, A. Becker, A. Zimmer, O. Brüstle, M. Peitz, M. Hemberger, H. Schorle, Derivation and maintenance of murine trophoblast stem cells under defined conditions. *Stem Cell Reports* **2**, 232–242 (2014). doi:10.1016/j.stemcr.2013.12.013 Medline
36. C. B. Park, D. Dufort, Nodal expression in the uterus of the mouse is regulated by the embryo and correlates with implantation. *Biol. Reprod.* **84**, 1103–1110 (2011). doi:10.1095/biolreprod.110.087239 Medline
37. G. J. Inman, F. J. Nicolás, J. F. Callahan, J. D. Harling, L. M. Gaster, A. D. Reith, N. J. Laping, C. S. Hill, SB-431542 is a potent and specific inhibitor of transforming growth factor-beta superfamily type I activin receptor-like kinase (ALK) receptors ALK4, ALK5, and ALK7. *Mol. Pharmacol.* **62**, 65–74 (2002). doi:10.1124/mol.62.1.65 Medline
38. Q. Wu, K. Kanata, R. Saba, C.-X. Deng, H. Hamada, Y. Saga, Nodal/activin signaling promotes male germ cell fate and suppresses female programming in somatic cells. *Development* **140**, 291–300 (2013). doi:10.1242/dev.087882 Medline
39. B. G. Herrmann, Expression pattern of the Brachyury gene in whole-mount TWis/TWis mutant embryos. *Development* **113**, 913–917 (1991). Medline
40. D. G. Wilkinson, S. Bhatt, B. G. Herrmann, Expression pattern of the mouse T gene and its role in mesoderm formation. *Nature* **343**, 657–659 (1990). Medline
41. H. J. Fehling, G. Lacaud, A. Kubo, M. Kennedy, S. Robertson, G. Keller, V. Kouskoff, Tracking mesoderm induction and its specification to the hemangioblast during embryonic stem cell differentiation. *Development* **130**, 4217–4227 (2003). doi:10.1242/dev.00589 Medline
42. A. Scialdone, Y. Tanaka, W. Jawaid, V. Moignard, N. K. Wilson, I. C. Macaulay, J. C. Marioni, B. Göttgens, Resolving early mesoderm diversification through single-cell expression profiling. *Nature* **535**, 289–293 (2016). doi:10.1038/nature18633 Medline
43. G. Peng, S. Suo, J. Chen, W. Chen, C. Liu, F. Yu, R. Wang, S. Chen, N. Sun, G. Cui, L. Song, P. P. Tam, J. D. Han, N. Jing, Spatial transcriptome for the molecular annotation of lineage fates and cell identity in mid-gastrula mouse embryo. *Dev. Cell* **36**, 681–697 (2016). doi:10.1016/j.devcel.2016.02.020 Medline
44. H. R. Schöler, G. R. Dressler, R. Balling, H. Rohdewohld, P. Gruss, Oct-4: A germline-specific transcription factor mapping to the mouse t-complex. *EMBO J.* **9**, 2185–2195 (1990). Medline
45. A. Ferrer-Vaquer, A. Piliszek, G. Tian, R. J. Aho, D. Dufort, A.-K. Hadjantonakis, A sensitive and bright single-cell resolution live imaging reporter of Wnt/ß-catenin signaling in the mouse. *BMC Dev. Biol.* **10**, 121 (2010). doi:10.1186/1471-213X-10-121 Medline
46. A. Niida, T. Hiroko, M. Kasai, Y. Furukawa, Y. Nakamura, Y. Suzuki, S. Sugano, T. Akiyama, DKK1, a negative regulator of Wnt signaling, is a target of the beta-catenin/TCF pathway. *Oncogene* **23**, 8520–8526 (2004). doi:10.1038/sj.onc.1207892 Medline
47. K. A. Lawson, N. R. Dunn, B. A. Roelen, L. M. Zeinstra, A. M. Davis, C. V. E. Wright, J. P. W. F. M. Korving, B. L. M. Hogan, Bmp4 is required for the generation of primordial germ cells in the mouse embryo. *Genes Dev.* **13**, 424–436 (1999). doi:10.1101/gad.13.4.424 Medline
48. U. Günesdogan, E. Magnúsdóttir, M. A. Surani, Primordial germ cell specification: A context-dependent cellular differentiation event. *Philos. Trans. R. Soc. Lond. B Biol. Sci.* **369**, 20130543 (2014). doi:10.1098/rstb.2013.0543 Medline
49. B. Payer, S. M. Chuva de Sousa Lopes, S. C. Barton, C. Lee, M. Saitou, M. A. Surani, Generation of stella-GFP transgenic mice: A novel tool to study germ cell development. *Genesis* **44**, 75–83 (2006). doi:10.1002/gene.20187 Medline
50. L. B. Zimmerman, J. M. De Jesús-Escobar, R. M. Harland, The Spemann organizer signal noggin binds and inactivates bone morphogenetic protein 4. *Cell* **86**, 599–606 (1996). doi:10.1016/S0092-8674(00)80133-6 Medline
51. T. Kunath, D. Arnaud, G. D. Uy, I. Okamoto, C. Chureau, Y. Yamanaka, E. Heard, R. L. Gardner, P. Avner, J. Rossant, Imprinted X-inactivation in extra-embryonic endoderm cell lines from mouse blastocysts. *Development* **132**, 1649–1661 (2005). doi:10.1242/dev.01715 Medline
52. K. K. Niakan, N. Schrode, L. T. Y. Cho, A.-K. Hadjantonakis, Derivation of extraembryonic endoderm stem (XEN) cells from mouse embryos and embryonic stem cells. *Nat. Protoc.* **8**, 1028–1041 (2013). doi:10.1038/nprot.2013.049 Medline
53. I. Bedzhov, C. Y. Leung, M. Bialecka, M. Zernicka-Goetz, *In vitro* culture of mouse blastocysts beyond the implantation stages. *Nat. Protoc.* **9**, 2732–2739 (2014). doi:10.1038/nprot.2014.186 Medline
54. S. Tanaka, Derivation and culture of mouse trophoblast stem cells in vitro. *Methods Mol. Biol.* **329**, 35–44 (2006). Medline
55. J. M. Rhee, M. K. Pirity, C. S. Lackan, J. Z. Long, G. Kondoh, J. Takeda, A.-K. Hadjantonakis, *In vivo* imaging and differential localization of lipid-modified GFP-variant fusions in embryonic stem cells and mice. *Genesis* **44**, 202–218 (2006). doi:10.1002/dvg.20203 Medline
56. G. Y. Lee, P. A. Kenny, E. H. Lee, M. J. Bissell, Three-dimensional culture models of normal and malignant breast epithelial cells. *Nat. Methods* **4**, 359–365 (2007). doi:10.1038/nmeth1015 Medline
57. E. Faure, T. Savy, B. Rizzi, C. Melani, O. Stašová, D. Fabrèges, R. Špir, M. Hammons, R. Čúnderlík, G. Recher, B. Lombardot, L. Duloquin, I. Colin, J. Kollár, S. Desnoulez, P. Affaticati, B. Maury, A. Boyreau, J. Y. Nief, P. Calvat, P. Vernier, M. Frain, G. Lutfalla, Y. Kergosien, P. Suret, M. Remešíková, R. Doursat, A. Sarti, K. Mikula, N. Peyriéras, P. Bourgine, A workflow to process 3D+time microscopy images of developing organisms and reconstruct their cell lineage. *Nat. Commun.* **7**, 8674 (2016). Medline
58. R Core Team, R: A language and environment for statistical computing. R Foundation for Statistical Computing, Vienna, Austria. URL http://www.R-project.org/ (2013).
59. GraphPad Prism version 7.00 for Windows, GraphPad Software, La Jolla California USA. *www.graphpad.com*

ACKNOWLEDGMENTS

We are enormously grateful to D. Glover, M. Shahbazi, S. Vuoristo and F. Antonica for helpful feedback on the manuscript; A. Hupalowska for drawing models (Fig. 1a; 2i and 8) and G. Recher for 3D rendering (Fig. 1b,d); the creators of the 'Bioemergences' platform for providing image analysis tools; V. Kuskoff, A. Surani, and B. Herrmann, for providing T:GFP ESCs, Stella:GFP ESCs. We are grateful to the Wellcome Trust and ERC for supporting this work. S.E.H and C.K are both supported by BBSRC Doctoral training partnership studentships. BS is supported by the International Research Fellowship Program 2214/A from Scientific and Technological Research Council of Turkey, and MZG by the Wellcome Trust. SEH served as an intern in the Cambridge, UK office of Science/AAAS. MZG and SEH are inventors on a patent application (1615343.9) submitted by Cell Guidance Systems, in which the University of Cambridge and the Wellcome Trust are beneficiaries, that covers the method and medium composition used to generate "stem cell-derived embryos." Author contributions: S.E.H and B.S carried out experiments and data analysis on ETS-embryos. N.C and C.K carried out experiments on natural embryos. M.Z.G conceived, supervised the study and wrote the paper with the help of S.E.H and B.S.

SUPPLEMENTARY MATERIALS
www.sciencemag.org/cgi/content/full/science.aal1810/DC1
Figs. S1 to S6
Tables S1 and S2

9 October 2016; accepted 17 February 2017
Published online 2 March 2017
10.1126/science.aal1810

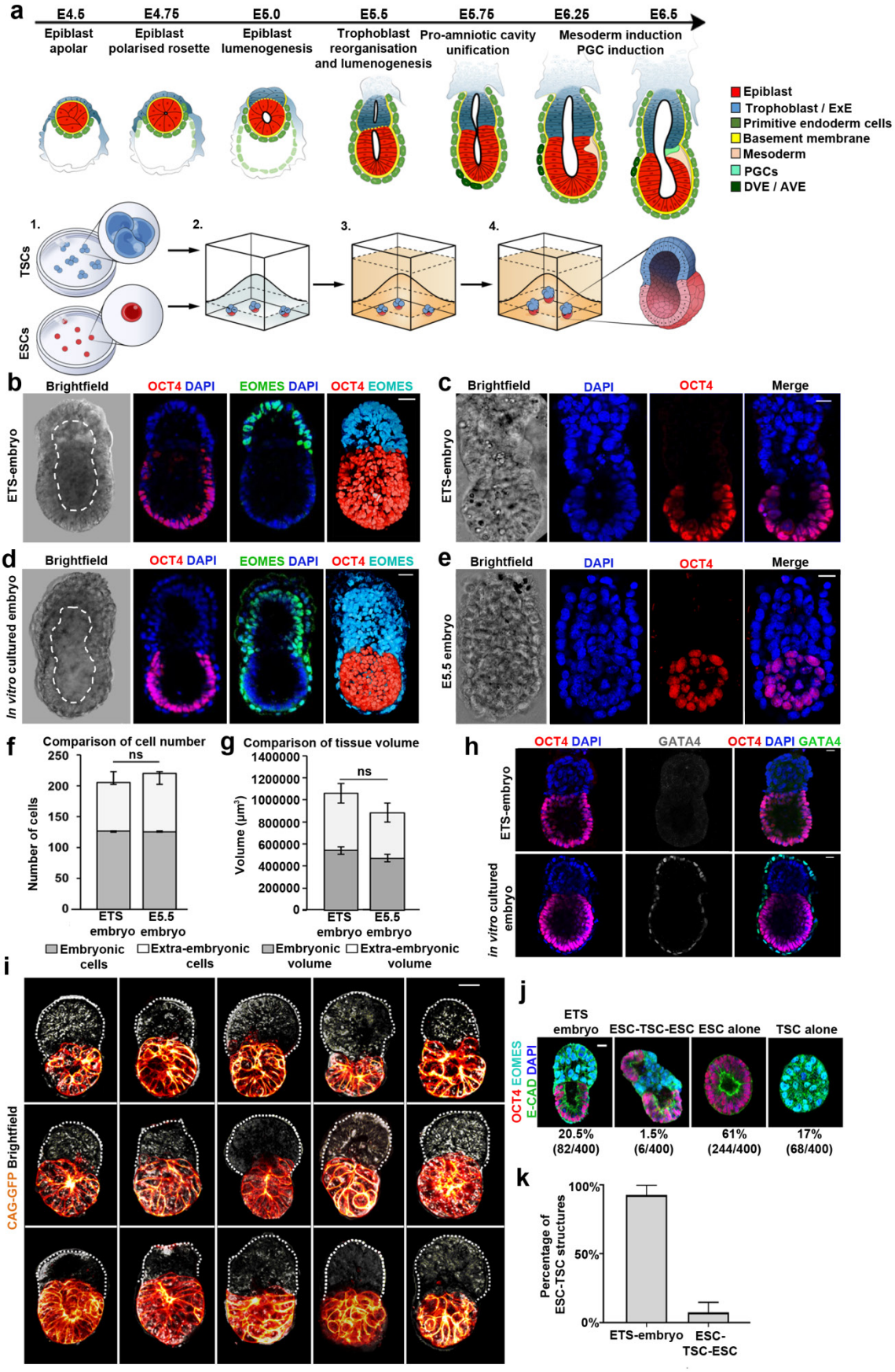

Fig. 1. Self-assembly of ESCs and TSCs into an ETS-embryo. a. Top: Development of the mouse embryo from the pre-implantation blastocyst to post-implantation egg cylinder and mesoderm specification. Red cells, epiblast; dark blue cells, trophectoderm/ extra-embryonic ectoderm; Green cells, primitive endoderm/visceral endoderm cells; Dark green cells, Distal/Anterior Visceral endoderm; Beige cells, mesodermal cells; Sea green cells, Primordial Germ Cells; yellow line, basement membrane. Bottom: Scheme of protocol to generate ETS-embryos. ESCs and TSCs cultured in standard conditions (1). Single ESCs and small clumps of TSCs suspended in 3D ECM of Matrigel, plated in drops and allowed to solidify (2), before culturing in ETS-embryo medium established for this purpose (3; Materials &Methods). Embryo-like structures emerge within 96 hours (4). **b.** ETS-embryo of size approximately 100µmx200µm after 96 hours of culture stained to reveal: Oct4, red; Eomes, green, embryonic and extra-embryonic markers respectively; DNA, blue; white line highlights cavity. Bar=20µm; n=20. Rightmost panel: 3D rendering of same ETS-embryo: Red, Oct4; Cyan, Eomes. **c**. ETS-embryo: Oct4, red; DNA, blue. Bar =20µm; n=20. **d**. Embryo cultured in vitro for 48 hours from the blastocyst stage: Oct4, red; Eomes, green; DNA, blue; white line highlights cavity; Bar= 20µm; n=20. Rightmost panel: 3D rendering of same in vitro cultured embryo: Oct4, red; Eomes, cyan. **e.** Post-implantation embryo recovered at E5.5: Oct4, red; DNA, blue. Bar =20µm; n=20. **f.** ETS-embryos have similar number of cells after 96 hours to natural embryos (cultured for 48 hours from the late blastocyst stage; equivalent to E5.5 embryos) in embryonic and extra-embryonic compartments (Student's *t* test, n=20 per group, (2 separate experiments; not significant). Error bars = SEM. **g.** Mean tissue volumes of embryonic and extra-embryonic parts are similar for ETS-embryos after 96 hours and natural embryos cultured for 48 hours in vitro from the late blastocyst stage (equivalent to E5.5 embryos). Student's *t* test, n=20 per group, 2 separate experiments; not significant. Error bars=SEM. NB: Volume occupied by the visceral endoderm was excluded from quantification in natural embryos. See Materials & Methods for how volume was calculated. **h.** Upper panels: ETS-embryo stained to reveal: Oct4, red; DNA, Blue; Gata4, grey/green. Bar = 20µm. n=10. Lower panels: In vitro cultured embryo for 48 hours from the late blastocyst stage: Oct4, red; DNA, Blue; Gata4, grey/green. n=30. Bar = 20µm. **i.** Examples of live ETS-embryos generated from one single typical experiment using CAG-GFP ESCs (Rhee *et al*., 2006) to mark embryonic compartment and wild-type TSCs after 96 hours. Orange, CAG-GFP; Black, Brightfield. Brightfield was false-colored with the 'edges' "Look-up-table" function in Fiji software. White dotted line marks the outside of the TSC compartment for clarity. Bar= 20µm. **j.** Frequency of ETS-embryos, "twin" (ESC-TSC-ESC) structures, and individual TSC or ESC structures in a representative experiment. Red, Oct4; green, E-cadherin, cyan, Eomes; blue, DNA. Bar=20µm. 100 structures counted per experiment; 4 separate experiments. **k.** Proportion of ESC- and TSC-structures that form ETS-embryos versus "twin structures". n=88; 4 separate experiments. Error bars= SEM.

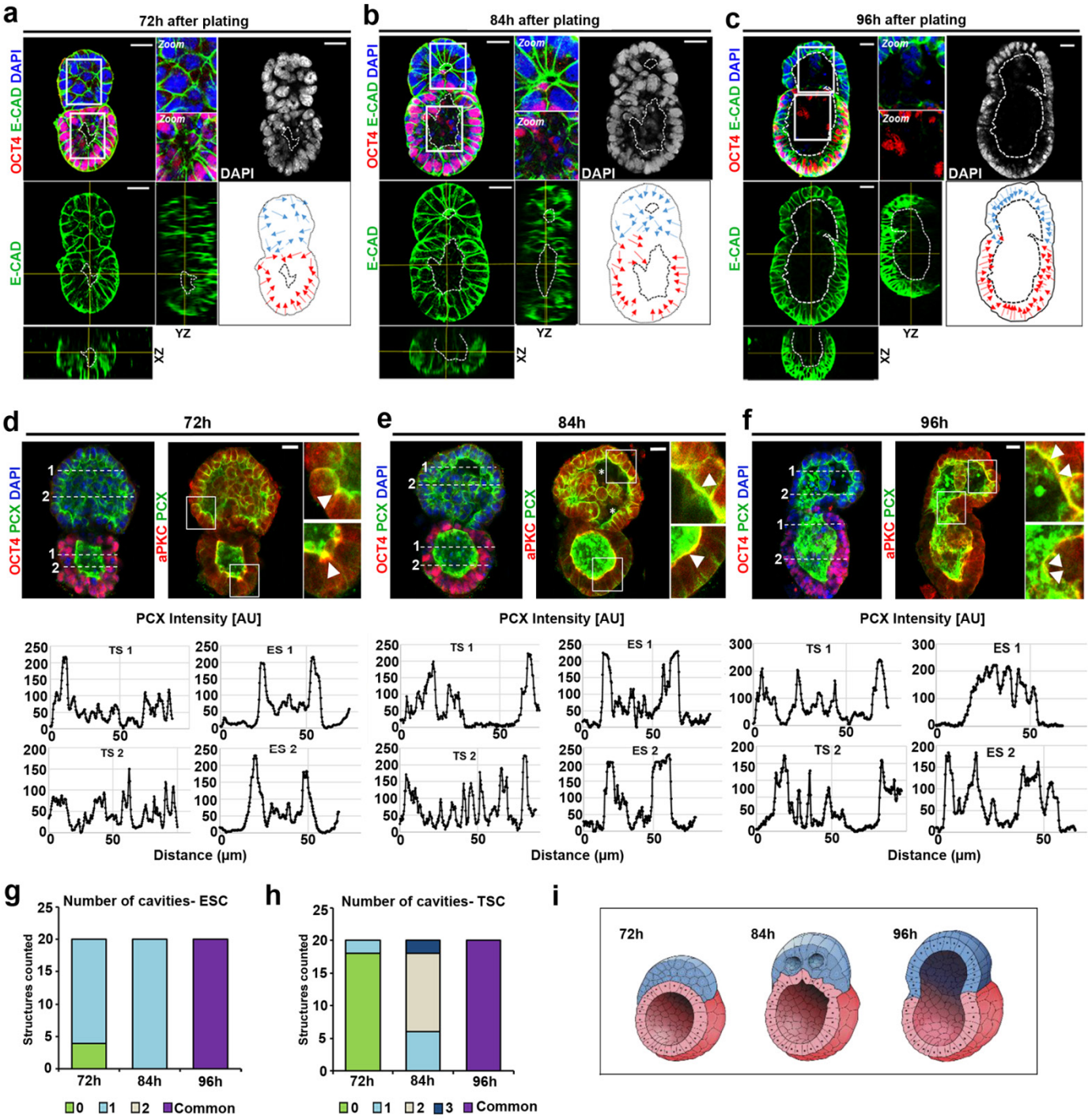

Fig. 2. Morphogenetic steps leading to cavitation of ETS-embryos are similar to natural embryos. a-c. ETS-embryos after 72, 84 and 96 hours showing progression of cavitation. Oct4, red; E-cadherin, green; DNA, blue/gray. Orthogonal views are shown for E-cadherin staining at each time-point. Zoomed fields highlight cavitated areas at each time-point; white or black dotted lines highlight cavities. Lower right panel for each time-point show orientation of nuclei in ESC compartments (red) and TSC compartments (blue) – nuclei become aligned to cavities; n=20 ETS-embryos per time-point, at least 2 separate experiments per time-point. Bar=20μm. **d-f**. ETS-embryos at three successive time-points during cavitation and intensity scans of PCX along indicated numerically labeled dashed white lines taken at middle z plane. PCX accumulates on the apical sides of cells (marked by aPKC) facing a lumen, so the presence of a cavity is indicated by two strong peaks in the intensity profile. Y-axis: PCX fluorescence intensity. Staining indicates Oct4/aPKC, red; PCX, green; DNA, blue. Bar=20μm. n=30, 3 separate experiments. Zoomed images indicate co-localisation of aPKC and PCX (white arrowheads). Asterisks indicate small cavities in the TSC compartment at 84 hours. **g-h.** Quantification of number of cavities in respective ESC- and TSC-compartments of ETS-embryos at 72, 84, and 96 hours. n=20 ETS-embryos analyzed per time-point. **i.** Schematics depicting "ETS-embryo" morphology during cavitation process at 72, 84, and 96 hours (red, embryonic compartment; blue, extra-embryonic compartment).

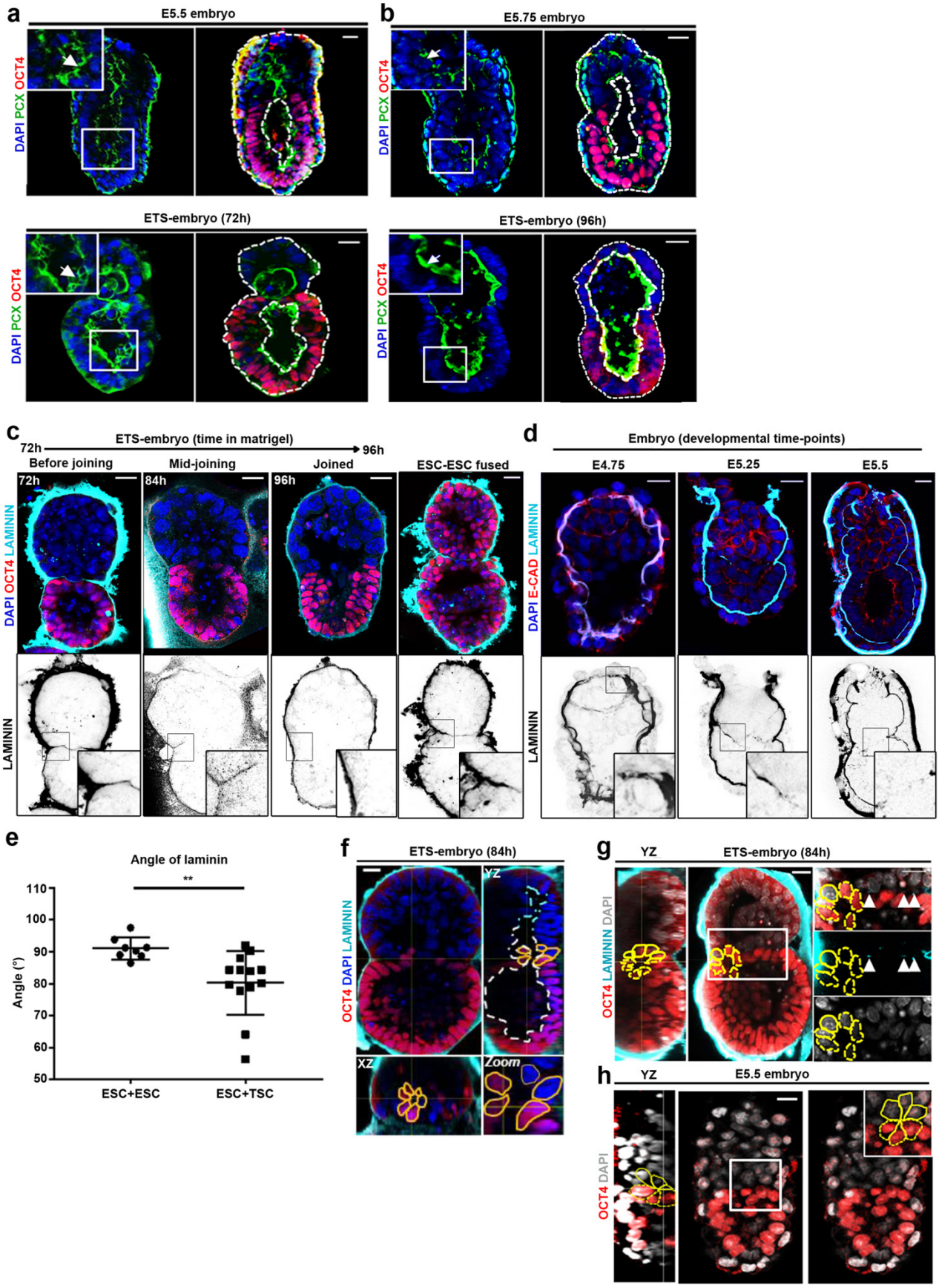

Fig. 3. Morphogenetic re-arrangement during cavity unification between embryonic and extra-embryonic compartments: a-b. Embryos at E5.5 and E5.75 (upper panels) and ETS-embryos at 72 and 96 hours (lower panels) stained to reveal Oct4, red; PCX, green; DNA, blue. Zoomed insets and white arrows highlight cavities; white dashed lines trace outlines of embryo and cavity in respective embryonic or ESC compartments or the common cavity at the later stage. Bar= 20μm. n=20 embryos or ETS-embryos each analyzed in at least 2 separate experiments. **c.** ETS-embryos during cavitation showing: Upper: Oct4, red; DNA, blue; laminin, cyan. Lower panel shows the laminin staining inverted for better contrast. Black boxes indicate the region of the zoomed inset. Bar =20μm; n=20, 2 separate experiments. Rightmost panel shows two fused ESC-structures after 84 hours. Inset shows residual laminin that is not broken down between the fusing compartments. n=8, 2 separate experiments. **d.** Peri-implantation embryos showing breakdown of basement membrane between embryonic and extra-embryonic compartments; Upper: E-cadherin, red; DNA, blue; laminin, cyan. Lower panel shows the laminin staining inverted for better contrast. Black boxes indicate the region of the zoomed inset. Bar=20μm. n=10 per stage, 2 separate experiments. **e.** Laminin is not displaced from the horizontal in ESC-ESC structures (n=8, mean angular displacement $\ominus$= 91.05°; pooled from 2 separate experiments) compared with ETS-embryos (n=13, mean angular displacement $\ominus$= 80.3°; pooled from 2 separate experiments). Student's *t* test, P<0.01, Error bars= SEM. For description of measurement of angular displacement, see Materials &Methods. **f.** ETS-embryo during cavitation after 84 hours of culture stained to reveal: Oct4, red; laminin, cyan; DNA, blue. XZ and YZ orthogonal views also shown. Yellow line outlines cells in chimeric arrangements; white dashed lines trace outline of the cavity. Bar= 20μm. n=15, 2 separate experiments. **g.** Another example of a ETS-embryo during cavitation at 84 hours. Oct4, red; laminin, cyan; DNA, gray. YZ orthogonal view also shown. White arrowheads indicate residual laminin. Yellow lines trace chimeric arrangements of embryonic (dotted) and extra-embryonic (solid) cells at boundary; n=15, 2 separate experiments. Bar= 20μm. **h.** E5.5 embryo. Oct4, red; DNA, gray. YZ orthogonal view also shown. Inset highlights chimeric cell arrangement at the boundary (yellow dotted line, embryonic cells; yellow solid line, extra-embryonic cells), n=10. Bar=20μm.

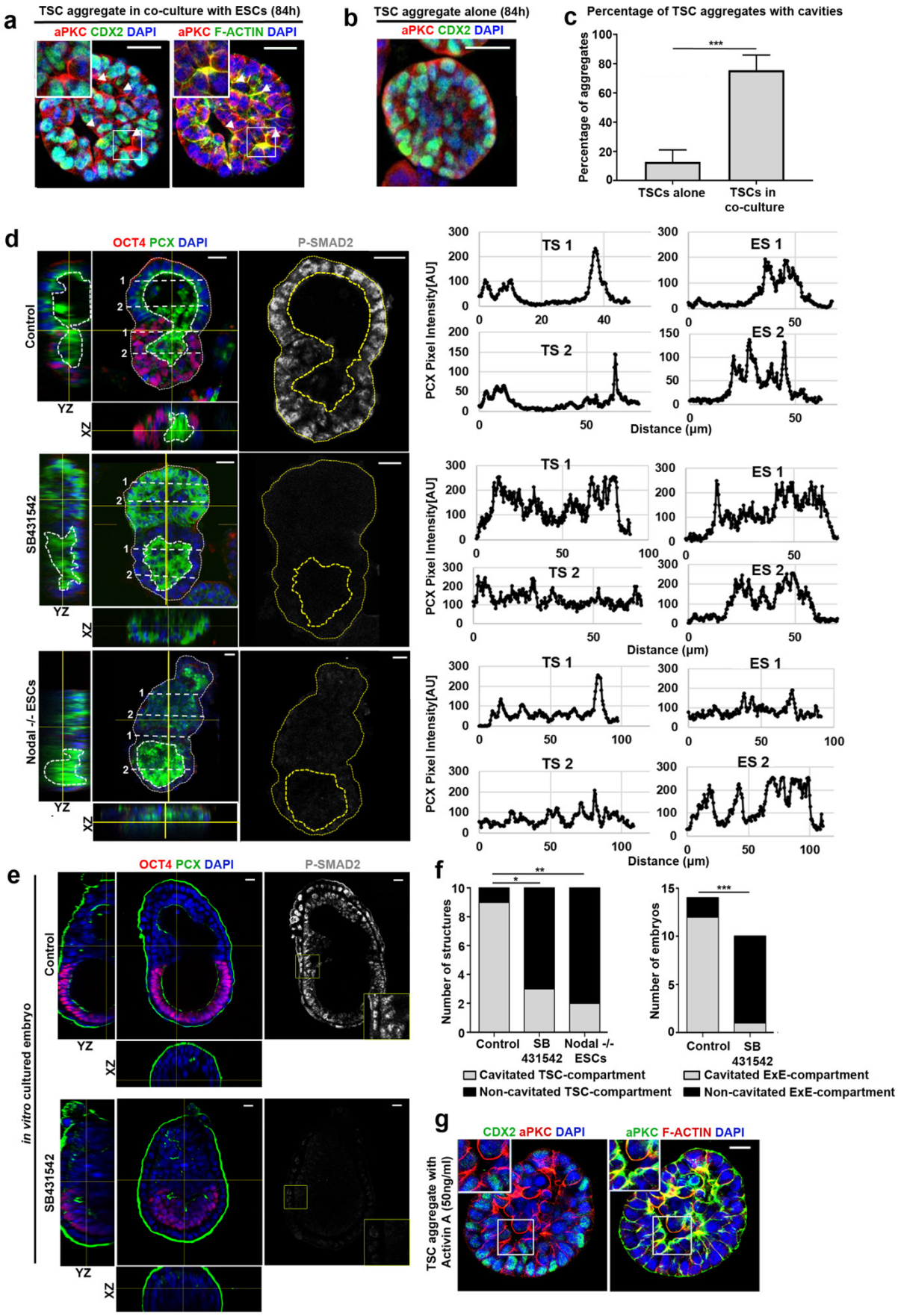

Fig. 4. Cavitation of the TSC compartment requires Nodal/Activin signaling. a. TSC aggregate at 84 hours in co-culture but not in contact with ESCs, Cdx2, green; DNA, blue; aPKC, red (left-hand panel) and F-actin, green; DNA, blue; aPKC, red (right-hand panel). White arrowheads indicate cavities. Zoomed inset displays a small cavity opening at a point of aPKC and F-actin enrichment. Bar= 30μm. n=20, 2 separate experiments. **b.** Sole TSC aggregate in 3D Matrigel at 84 hours. Cdx2, green; DNA, blue; aPKC, red. No cavities could be detected and aPKC is not polarised. n=20 structures analyzed that all displayed this morphology, 2 separate experiments. Bar=30μm. **c.** Quantitation of cavitation in TSC- aggregates cultured either alone or in the presence of ESCs for 84 hours. n=10 structures counted per condition per experiment; 2 separate experiments. Student's *t* test, P<0.001. **d.** ETS-embryos built from either control or *Nodal −/−* ESCs or cultured in 10μM SB431542 for 96 hours: Oct4, red; PCX, green; DNA, blue; P-SMAD2, grey. Bar=20μm. White/ Yellow dashed lines highlight outline of ETS-embryo and cavity. XZ and YZ orthogonal views highlight cavity where present. Fluorescence traces are of PCX intensity along region indicated by the numbered dotted lines in the ESC and TSC compartments. n=10. **e.** Embryos recovered at E5.0 and cultured in vitro for 36 hours in control (DMSO; n=14, 3 separate experiments) or in the presence of SB431542 (10μM; n=10, 3 separate experiments). Oct4, red; PCX, green; DNA, blue; P-SMAD2, grey. Inset highlights P-SMAD2 staining in the extra-embryonic ectoderm in each case. Bar= 50μm. **f.** Left panel: Quantification showing the number of ETS-embryos with cavitated TSC compartments after 96 hours in culture in control, SB431542 and Nodal−/− ESC conditions. n=10 per group, 2 separate experiments. Count data are presented as a bar chart, and a contingency table was used to perform the statistical test. Fisher's exact test, P<0.05. Right panel: Quantification showing the number of embryos with cavitated extra-embryonic compartments when recovered at E5.0 and cultured for 36 hours in control (n=14) or SB431542 (n=10) conditions, 2 separate experiments. Count data are presented as a bar chart, and a contingency table was used to perform the statistical test. Fisher's exact test, P<0.001. **g.** TSC aggregate cultured in 50ng/ml Activin A for 72 hours (left-hand panel) Cdx2, green; DNA, blue; aPKC, red. (right-hand panel): F-actin, green; DNA, blue; aPKC, red. Zoomed inset displays small cavity opening where aPKC and F-actin are enriched. Bar=50μm. n=20, 3 separate experiments.

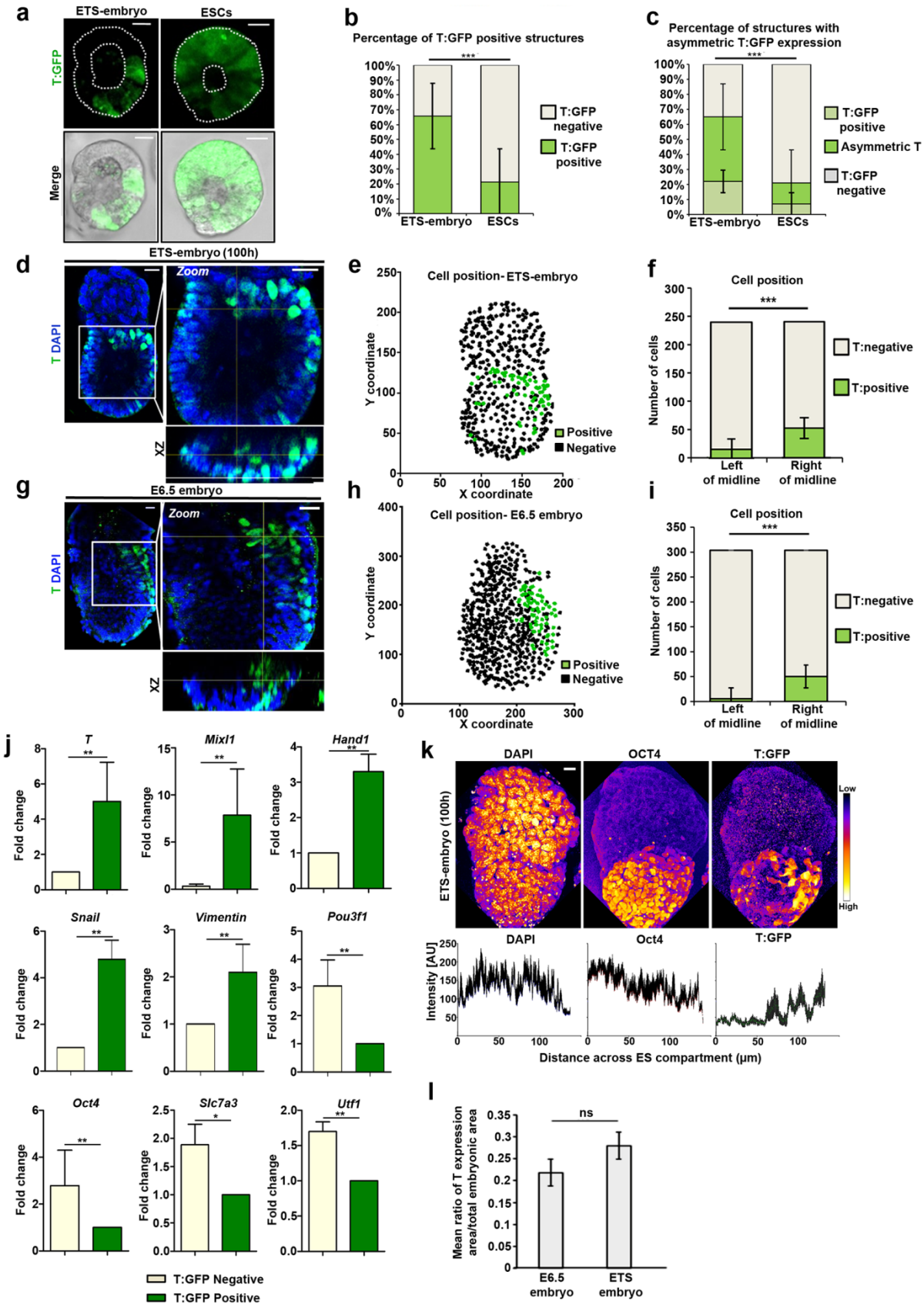

Fig. 5. ETS-embryos develop to express mesoderm markers a. *T/Brachyury:GFP*-expressing ESCs (green) growing alone (right) or as part of a ETS-embryo (left) in Matrigel. Bar=20μm; white dotted lines outline each structure and its cavity. n=100 "ETS-embryos", 4 experiments; n=65 ESC-alone structures, 4 experiments. **b.** Proportion of ETS-embryos expressing *T:GFP* at 96 hours is significantly higher in comparison to ESCs-alone structures. Fisher's exact test, P<0.001, n=108: 64 ETS-embryos and 44 ESC-alone structures counted in 2 separate experiments. Error bars=SEM. **c.** Proportion of *T/Brachyury* expressing ETS-embryos or -structures comprising only ESCs with asymmetric domain of *T/Brachyury* expression with respect to the long axis (equivalent to the midline) of the structure (Methods). Student's *t* test, P<0.001, n=100 ETS-embryos and n=100 structures comprising only ESCs per experiment. Mean of 4 separate experiments, Error bars= SEM. **d-f.** Quantitative assessment of endogenous *T* asymmetry in a ETS-embryo at 100 hours (**d**) revealing *T*, green; DNA, blue. Zoomed inset highlights T/Brachyury-expressing region; XZ panel highlights asymmetry in T/Brachyury to one side of structure. Bar=20μm. Projection of all cell coordinates in 2D (**e**): black points, T negative cells; green points, T positive cells. Proportion of T-positive versus T-negative cells around mid-line, equivalent to the long axis of each structure (**f**; Methods). Fisher's exact-test, P<0.001. Error bars=SEM. **g-i.** Quantitative assessment of *T* asymmetry in E6.5 natural embryo (**g**) revealing T, green and DNA, blue. Zoomed inset highlights T/Brachyury-expressing region; XZ panel, asymmetry in T/Brachyury. Bar=20μm. Projection of cell coordinates (**h**) as in panel (**e**). Proportion of T-positive versus T-negative cells around mid-line, long axis of each structure (**i**). Fisher's exact-test, P<0.001. Error bars=SEM. **j.** RT-qPCR analysis of the expression of mesodermal markers (*T, Mixl1* and *Hand1),* epithelial-to-mesenchymal transition (EMT) markers (*Snai1* and *Vimentin)* and markers known to be elevated in the region opposite to the mesoderm region of the E6.5 embryo *(Pou3f1, Oct4, Slc7a3,* and *Utf1)*in T:GFP positive cells of a ETS-embryo (collected after 100 hours in culture) compared with T:GFP negative cells from the ESC compartment of the same structure. Mesodermal and EMT marker expression was significantly increased in T:GFP positive cells, while cell markers known to be elevated in the region opposite the mesoderm region were significantly decreased. Student's *t* test, P<0.05. N=4 biological replicates. Error bars= SEM. Note that for *Mixl1,* gene expression in some samples of T:GFP-negative cells were undetermined, and so were accepted as zero. **k.** Top: A ETS-embryo after 100 hours immunostained to reveal: DNA, left; Oct4, middle; and T:GFP, right. Images are maximum projections and are false-colored with the 'fire' "Look-up table" function in Fiji software to highlight intensity gradients. Bar=20μm. Bottom: mean intensity profiles for immunofluorescence stainings plotted as the mean +/− SEM for eight different cross-sections of the embryonic compartment of the ETS-embryo shown. **l.** Comparable size of T expression in ETS-embryos and E6.5 embryos. n=10 per group, Mean ratio of areas of mesodermal domain/total epiblast in E6.5 embryo. Student's *t* test, not significant, error bars= SEM. For a description of how the ratio was measured and calculated, see Materials & Methods..

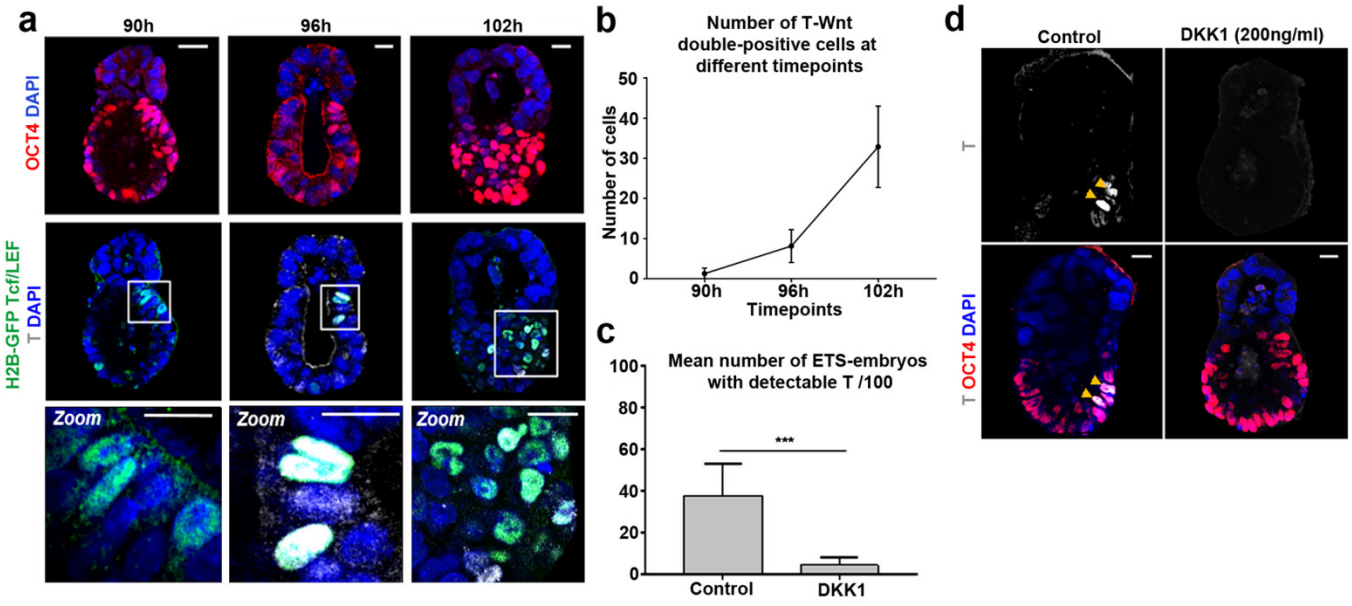

Fig. 6. ETS-embryos express mesoderm markers in response to Wnt signaling. a. ETS-embryos expressing the Wnt reporter H2B-GFP:Tcf/LEF and *T/Brachyury* at 90, 96, and 102 hours of culture. Oct4, red; DNA, blue; H2B-GFP:Tcf/LEF, green; T/Brachyury, white. Bar=20μm. Inset (Bar=10μm) highlights cells co-expressing Wnt reporter and T/Brachyury. n=15 per each time-point. **b.** Quantification of mean number of Wnt/Brachyury co-expressing cells detected in the ESC compartment of ETS-embryos with time. The number of cells is significantly different in each group (ANOVA test, $P<0.01$). n=15 per time-point, 3 separate experiments. Error bars=SEM. **c.** Proportion of ETS-embryos expressing T/Brachyury is reduced in presence of DKK1 (200ng/ml) compared to controls. Student's *t* test, $P<0.001$, n=400, 4 separate experiments. **d.** Representative ETS-embryos cultured in 200ng/ml DKK1 and control conditions for 96 hours. Oct4, red; DNA, blue; T/Brachyury, white. Yellow arrows indicate T/Brachyury-positive cells in control conditions, undetectable in DKK1 conditions. Bar= 20μm.

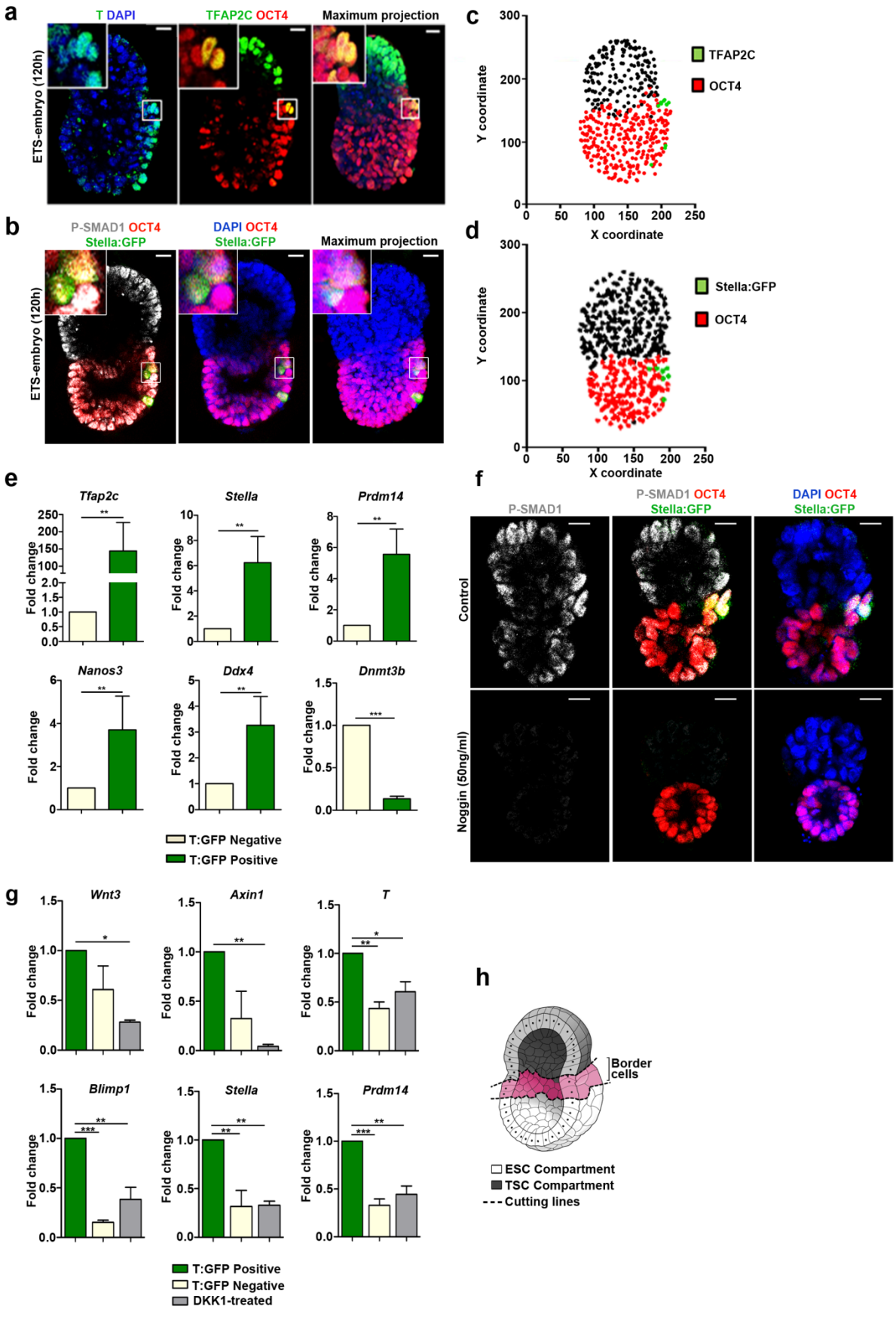

Fig. 7. ETS-embryos express primordial germ cell (PGC) markers in response to BMP signaling. a. ETS-embryo at 120 hours showing asymmetric expression of mesoderm and PGCs markers. Oct4, red; T/Brachyury, green; Tfap2c, green; and DNA, blue. Insets highlight the Oct4-Tfap2c double-positive cells which occupy the boundary in the T/Brachyury-positive region. Bar= 20μm. n=13, 2 separate experiments. Maximum projection shows merge of Tfap2c-Oct4-DAPI. **b.** ETS-embryo at 120 hours expressing Stella:GFP (green) concomitantly with p-SMAD1 (gray). Oct4, red; DNA, blue. Bar=20μm. n=15, 3 separate experiments. Insets highlight Stella:GFP-positive cells in ESC compartment. Maximum projection shows merge of Stella:GFP-Oct4-DAPI. **c.** Projected cell coordinates for the same ETS-embryo as in (a): black points, Oct4 and Tfap2c negative cells; Red points; Oct4 positive, Tfap2c negative cells; green points, Oct4 and Tfap2c double positive cells. **d.** Projected cell coordinates for same ETS-embryo as in (b). Black points, Stella:GFP and Oct4 negative cells; red points, Oct4-positive and Stella:GFP negative cells; green points, Oct4- and Stella:GFP positive cells. **e.** RT-qPCR analysis of the expression of PGC markers in ETS-embryo. *Tfap2c, Stella, Prdm14, Nanos3, Ddx4* and *Dnmt3b* in T:GFP positive and T:GFP negative cells from the same ETS-embryos collected after 120 hours in culture. Expression of PGC markers is significantly increased in T:GFP positive cells, Student's *t* test, $P<0.05$. n=5 biological replicates. Error bars= SEM. **f**. ETS-embryos at 96 hours cultured in control conditions or with BMP antagonist Noggin (50ng/ml). Oct4, red; DNA, blue; P-SMAD1, grey; Stella-GFP, green. Bar=20μm. n=15, 2 separate experiments. **g.** RT-qPCR analysis of the expression of PGC markers in 'border cells' collected from ETS-embryos in the presence of DKK1 (200ng/ml) versus T:GFP positive / negative cells collected from ETS-embryos in control conditions (collected after 120 hours in culture). Expression of PGC markers (*Blimp1*, *Stella,* and *Prdm14*) is significantly increased in T:GFP positive cells in control conditions, but this effect is abrogated when DKK1 is introduced into culture conditions . ANOVA followed by Tukey test. $P<0.05$. n=4 biological replicates. Error bars= SEM. We confirmed inhibition of the Wnt pathway by DKK1 by analysis of the expression of *Axin1*, *Wnt3* and *T* in all samples. **h**. Schematic representation of a ETS-embryo (ESC compartment white and TSC compartment grey) to illustrate where 'border cells' were dissected from in DKK-treated samples for RT-qPCR analysis.

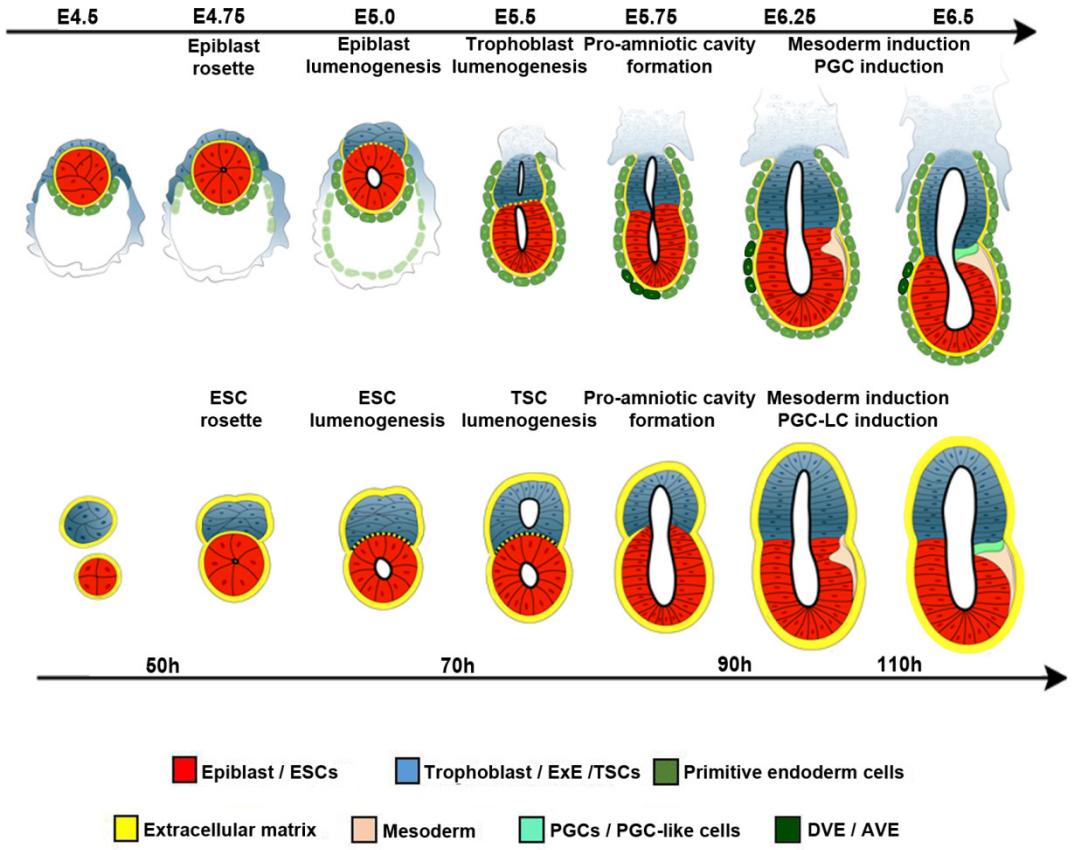

Fig. 8. ETS-embryos as a simplified model of embryo development from the blastocyst stage till mesoderm specification post-implantation. Comparison of development of natural and "ETS-embryos" mouse embryos. Red cells, ESC/epiblast; dark blue cells, TSC/trophectoderm/ extra-embryonic ectoderm cells; beige cells, mesoderm cells; Seagreen cells, Primordial Germ Cells; yellow line, basement membrane/ECM. In the embryo, Green cells are primitive endoderm/visceral endoderm cells; Dark green cells, Distal/ anterior Visceral Endoderm. The ETS-embryo is surrounded by ECM in similar manner to basement membrane of visceral endoderm in natural embryo. Mesoderm-expression domain is similarly positioned and occupies similar area of the embryonic compartment in both ETS-embryos and natural embryos.

Assembly of embryonic and extra-embryonic stem cells to mimic embryogenesis in vitro

Sarah Ellys Harrison, Berna Sozen, Neophytos Christodoulou, Christos Kyprianou and Magdalena Zernicka-Goetz (March 2, 2017)

published online March 2, 2017

Editor's Summary

Science (print ISSN 0036-8075; online ISSN 1095-9203) is published weekly, except the last week in December, by the American Association for the Advancement of Science, 1200 New York Avenue NW, Washington, DC 20005.